ABLATION AND VISCOUS EFFECTS ON THE FORCE AND MOMENT CHARACTERISTICS OF SLENDER CONE MODELS AT MACH 10 UNDER LAMINAR FLOW CONDITIONS

VON KÁRMÁN GAS DYNAMICS FACILITY
ARNOLD ENGINEERING DEVELOPMENT CENTER
AIR FORCE SYSTEMS COMMAND
ARNOLD AIR FORCE STATION, TENNESSEE 37389

October 1975

Final Report for Period July 1, 1973 — January 31, 1975

Prepared for

DIRECTORATE OF TECHNOLOGY
ARNOLD ENGINEERING DEVELOPMENT CENTER
ARNOLD AIR FORCE STATION, TENNESSEE 37389

This report has been reviewed by the Information Office (OI) and is releasable to the National Technical Information Service (NTIS). At NTIS, it will be available to the general public, including foreign nations.

APPROVAL STATEMENT

This technical report has been reviewed and is approved for publication.

FOR THE COMMANDER

ELTON R. THOMPSON
Research and Development
   Division
Directorate of Technology

ROBERT O. DIETZ
Director of Technology

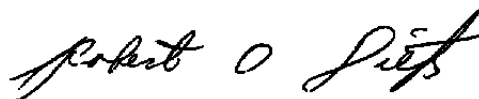| REPORT DOCUMENTATION PAGE		READ INSTRUCTIONS BEFORE COMPLETING FORM
1. REPORT NUMBER AEDC-TR-75-109	2. GOVT ACCESSION NO.	3. RECIPIENT'S CATALOG NUMBER
4. TITLE (and Subtitle) ABLATION AND VISCOUS EFFECTS ON THE FORCE AND MOMENT CHARACTERISTICS OF SLENDER CONE MODELS AT MACH 10 UNDER LAMINAR FLOW CONDITIONS		5. TYPE OF REPORT & PERIOD COVERED Final Report, July 1, 1973 to Jan 31, 1975
		6. PERFORMING ORG. REPORT NUMBER
7. AUTHOR(s) B. J. Griffith, W. T. Strike, and B. M. Majors, ARO, Inc.		8. CONTRACT OR GRANT NUMBER(s)
9. PERFORMING ORGANIZATION NAME AND ADDRESS Arnold Engineering Development Center (DY) Arnold Air Force Station, Tennessee 37389		10. PROGRAM ELEMENT, PROJECT, TASK AREA & WORK UNIT NUMBERS Program Element 65807F
11. CONTROLLING OFFICE NAME AND ADDRESS Arnold Engineering Development Center (DYFS), Arnold Air Force Station, Tennessee 37389		12. REPORT DATE October 1975
		13. NUMBER OF PAGES 34
14. MONITORING AGENCY NAME & ADDRESS(if different from Controlling Office)		15. SECURITY CLASS. (of this report) UNCLASSIFIED
		15a. DECLASSIFICATION/DOWNGRADING SCHEDULE N/A

16. DISTRIBUTION STATEMENT (of this Report)

Approved for public release; distribution unlimited.

17. DISTRIBUTION STATEMENT (of the abstract entered in Block 20, if different from Report)

18. SUPPLEMENTARY NOTES

Available in DDC.

19. KEY WORDS (Continue on reverse side if necessary and identify by block number)

conical bodies
models
slender bodies
dimensional viscous flow program
ablation
hypersonic wind tunnels

20. ABSTRACT (Continue on reverse side if necessary and identify by block number)

A comprehensive wind tunnel investigation was conducted in AEDC Tunnel C at Mach number 10 on 4- and 5-deg half-angle cones in order to study ablation and viscous effects under laminar flow conditions. Attention was focused on (1) the mode of ablation simulation, (2) obtaining consistent pitch plane force measurements in the angle-of-attack range from 0 to 4 deg, (3) the effect of bluntness, and (4) viscous effects over as large a

DD ₁FORM JAN 73 1473   EDITION OF 1 NOV 65 IS OBSOLETE

20. ABSTRACT (Continued)

Reynolds number range as possible utilizing Tunnel C. The subliming ablator used was camphor, which is compared to "blowing" through a porous surface using (1) nitrogen, (2) argon, and (3) sulphur hexafluoride (SF_6) gases. The study shows small differences in data from the two modes of ablation simulation using the 5-deg cone and significant viscous effects on both the static stability and drag characteristics of the 4-deg half-angle cone.

AFSC
Arnold AFS Tenn

PREFACE

1

CONTENTS

ILLUSTRATIONS

3

1.0 INTRODUCTION

Ablation and viscous effects on the force and moment characteristics of slender cones are not well understood. This report is the first in a planned series that will address these problems.

Ablation is generally simulated in the wind tunnel by injecting gas through the surface of a porous model. This mode of ablation simulation has many advantages over low-temperature ablators and so is an attractive technique. However, an experimental and analytical comparison of transpirationally cooling a model as opposed to using a subliming low-temperature ablator (camphor) has not been made on an identical model. This report presents a direct experimental and analytical comparison between the two modes of ablation simulation on the force and moment data of a sharp 5-deg cone at Mach number 10 under laminar flow conditions. The model was fabricated to allow testing with a solid steel, a porous shell, or a camphor sleeve with only minor model configuration changes. In order to separate the influence of molecular weight, a wide range of gases was utilized. These were SF_6 (sulphur hexafluoride), argon, and nitrogen, which have molecular weights of 146, 40, and 28, respectively. The molecular weight of the camphor was 152. The model was injected into the tunnel at zero angle of attack for a few seconds and pitched in a continuous-sweep mode to over 3 deg angle of attack and back to zero at a rate of approximately 1 deg per second. These data were taken at a free-stream Reynolds number of 1.0×10^6 per foot.

Solid steel, solid camphor, and partial camphor models with a nose-to-base bluntness ratio of 0.05 and a 4-deg half angle were also tested over a free-stream Reynolds number range from 0.302×10^6 to 2.03×10^6 per foot. The camphor model pieces were weighed before and after each run, and the time exposed to the flow was recorded. Other nose-to-base-bluntness ratios were also tested on the all-steel model. Figure 1a is a photograph of the 4-deg cone model installed in Tunnel C. A sketch showing the sting arrangement of the 5-deg cone model is shown in Fig. 1b. This arrangement provided minimal interference of the sting on the base pressure.

2.0 APPARATUS AND PROCEDURE

2.1 WIND TUNNEL

Tunnel C is a closed-circuit hypersonic wind tunnel with a 50-in.-diam test section and an axisymmetric contoured nozzle which provides a nominal Mach number of 10 over a range of pressure levels from 175 to 2,000 psia. Stagnation temperatures sufficient to avoid air liquefaction in the test section (up to 2,000°R) are maintained at all conditions. The tunnel is equipped with a model injection system, which allows removal of the model from the test section while the tunnel is in operation.
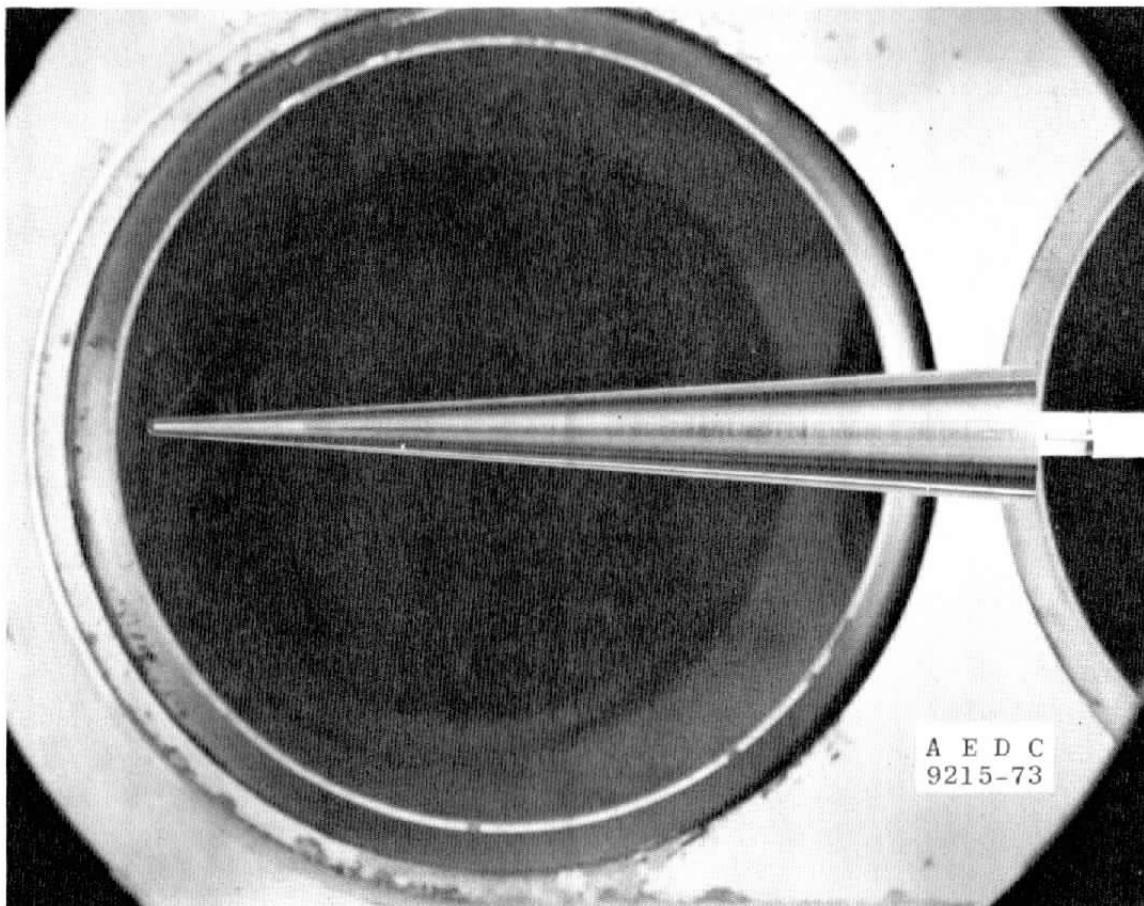
a. Photograph of basic 4-deg model, $R_N/R_B = 0.08$
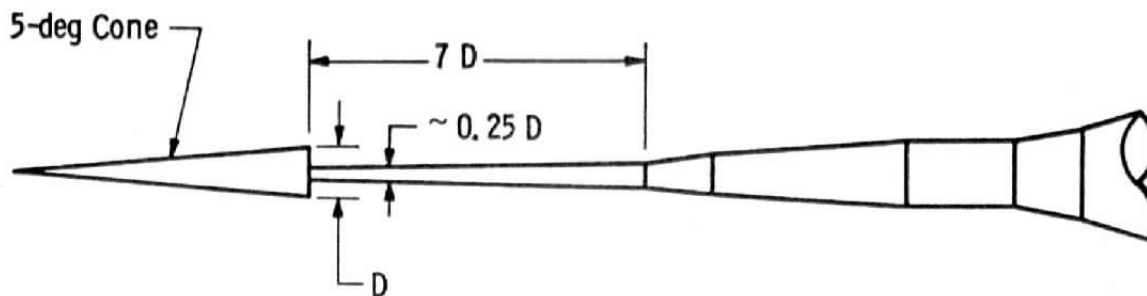
b. Schematic of 5-deg cone model
Figure 1. Models installed in Tunnel C.

2.2 MODELS

2.2.1 Sharp 5-deg Cone Model

A 5-deg half-angle cone model, 21-in. long with a 3.68-in. base diameter, was designed and fabricated for these experiments (see Fig. 2). The model was fabricated with an interchangeable steel nose section, rear frustrum, and steel base plate which permitted testing a solid steel frustrum or camphor frustrum and a porous sintered metal section.

	Configuration	L	L_1	D	L_1/L	A	B
Model 1	Steel or Camphor	21.003	14.219	3.675	0.6770	0.266	0
Model 2	Porous	21.029	14.237	3.680	0.6770	0.188	0.281

L ⎱ Used for Force and
D ⎰ Moment Coefficients

Figure 2. 5-deg sharp cone test model.

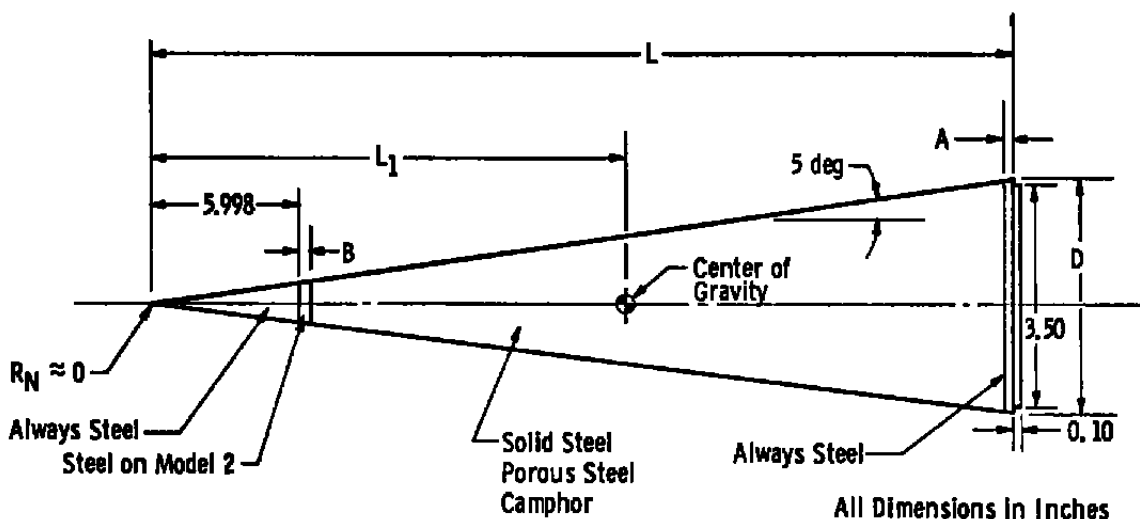Figure 3 shows the computed distribution of ablation along the camphor surface ($a = 0$) relative to a uniform ablation rate. A gross calibration of the porous frustrum is also given in Fig. 3. The normalized values given at each station represent the measured flow rate at that location on the model surface relative to a calculated flow for uniform blowing. This distribution was obtained by the General Electric Company (GE) and checked at AEDC using a hot-wire probe. It is very difficult to build into a porous model the distribution one would like to have, which is one of the primary disadvantages of this mode of ablation simulation. The influence of this type of distribution on the zero lift axial force can be computed. However, the influence on the static stability of the model is not easily predicted. A laminar boundary layer presumably would be more sensitive to fluctuations in the upstream history of the mass injection than would a turbulent boundary layer.

7
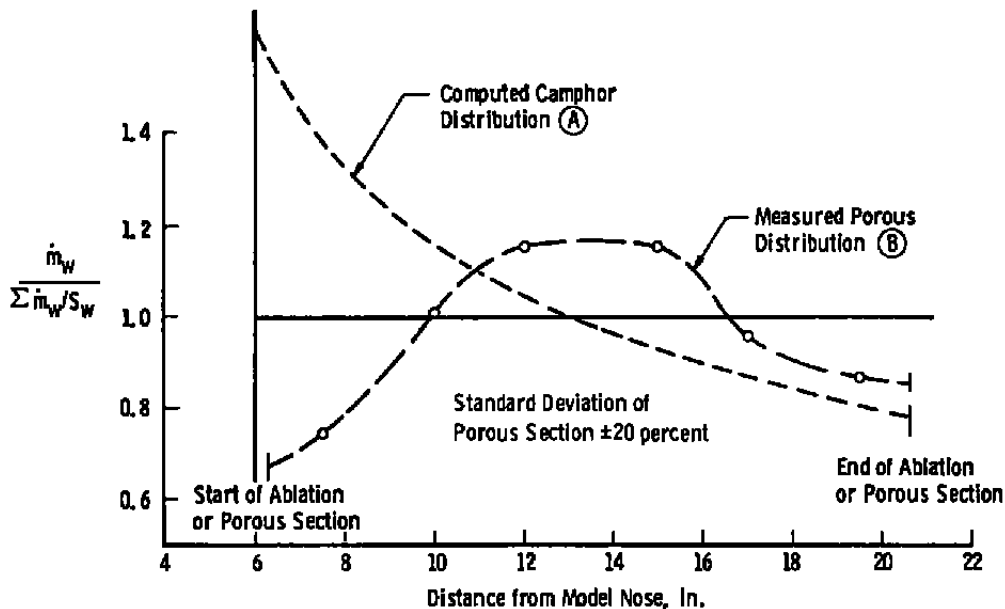
Figure 3. Relative axial distribution of camphor or porous model.

2.2.2 Basic 4-deg Cone Model

A 4-deg half-angle cone model, 17.875-in. long with a 2.5-in. base diameter, was also designed and fabricated. Steel noses with tips varying from sharp to $R_N/R_B = 0.224$ were built and tested. Camphor noses ($R_N/R_B = 0.05$), frustrums, and aft rings were constructed so that testing of an all-camphor model or all-steel model was possible. The basic model sketch is shown in Fig. 4. Figure 5 shows a photograph of the various parts of the all-steel model.
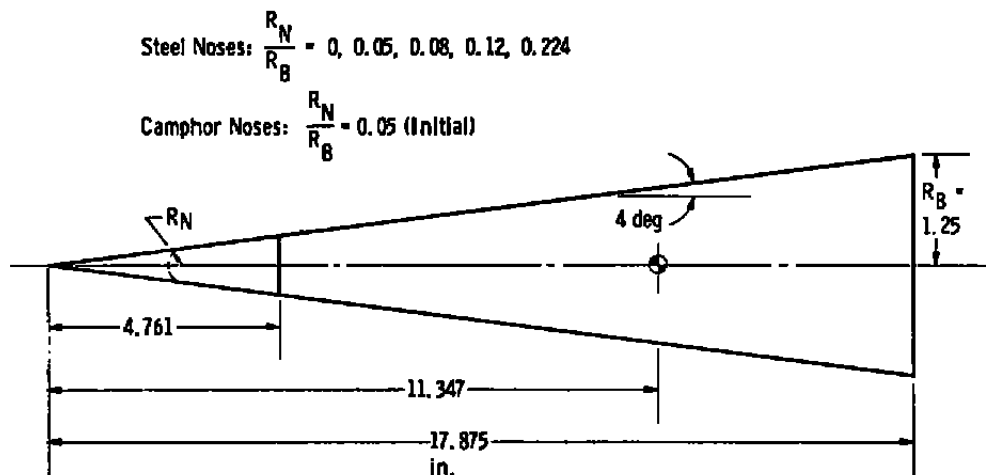
Figure 4. Basic 4-deg cone test model.
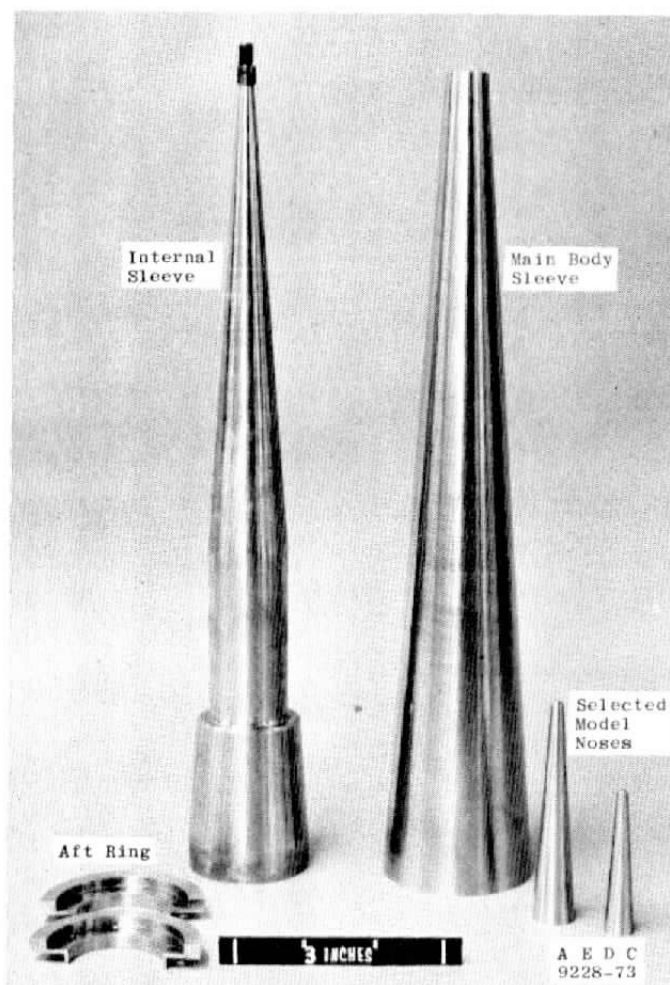
Figure 5. Photograph of steel 4-deg model.

2.3 BALANCE AND DATA PRECISION

A special three-component force balance (VKF Bal. No. 4.00-Y-23-066) was designed and fabricated for this test program. The original design criteria for this balance were as follows: the balance was to measure normal force loads up to 9 lbf to within 0.01 lbf and axial forces up to 1.5 lbf to within 0.003 lbf, and pass mass flow rates up to 0.010 lbm/sec with bellows pressure of less than 200 psia. As shown in Fig. 6, the mass flow line (a 0.125-in.-OD tube) passes through the forward and aft axial members of the balance. The gas supply then enters a small bellows section, and from there the gas passes through ten 0.063-in.-diam holes into a manifold. There is a bellows section on either side of this section of the 0.125-in.-diam gas supply line to minimize the influence of the mass flow system on the balance performance. A water jacket encloses the balance to keep the balance temperature within operational limits.
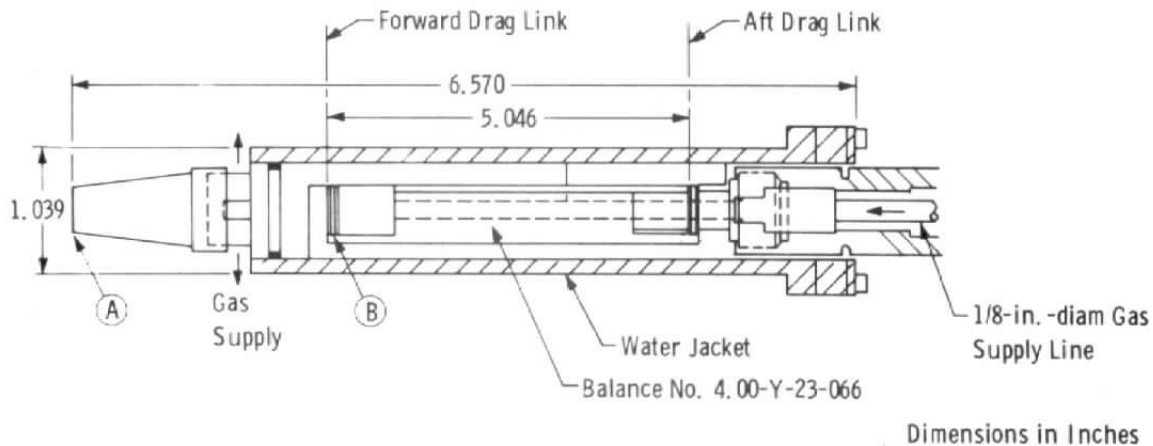
a. **Balance**

View Twice Size
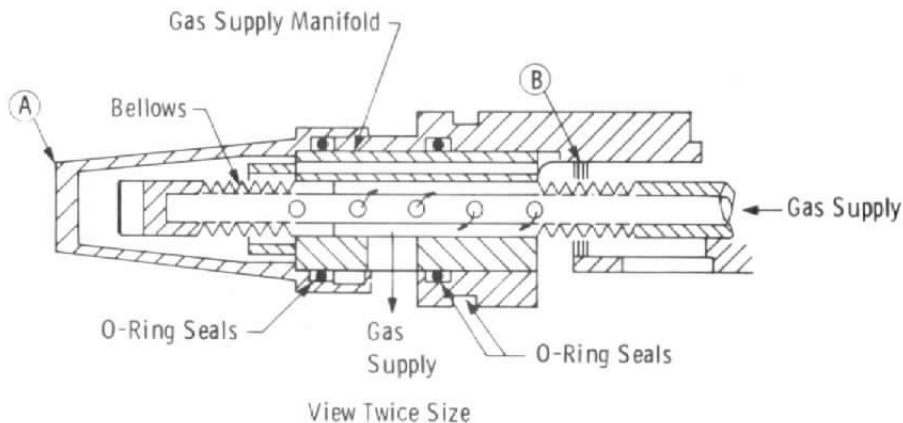
b. **Mass addition bellows system**
Figure 6. Three-component mass addition balance.

The actual performance of the balance follows; the uncertainties shown represent the measurement residuals which bracket 95 percent of the data, which represents the differences between the applied loads and the loads calculated from the balance calibration equations used in the final data reduction.

Balance Repeatability

Component	Units	Gas Supply On	Gas Supply Off
Normal Force	lbf	±0.029	±0.008
Pitching Moment	in.-lbf	±0.103	±0.015
Axial Force	lbf	±0.010	±0.003

10

The balance performance met the original design criteria with the mass flow system disconnected; however, the presence of the gas supply (i.e., pressure in the mass flow line) reduced the balance performance so that the uncertainty in the force measurements increased by a factor of about 5, as noted. An overall repeatability of the data from run to run and tunnel entry to tunnel entry is given below.

p_o, psia	C_N	C_m	C_{AT}	C_A
175	±0.0010	±0.0015	±0.002	±0.0025
1,500	±0.0007	±0.0010	±0.001	±0.0015

2.4 TEST TECHNIQUES

As a result of the nature of the models, the sensitivity of the specially designed balance, and the test requirements, nonstandard test procedures for wind tunnel force measurements were employed. Since some of the models used in the test programs ablated with time when exposed to an air stream, it was necessary to restrict this time of exposure in the air stream to less than a minute. The sensitivity of the balance output and the adverse model vibration produced by the tunnel operation required that electrical filters be imposed on the balance electrical responses. Also, the presence of a mass flow or pressurized bellows system in the balance which affected the zeros and repeatability of the balance imposed additional restrictions on the testing technique. Finally, the obvious test requirement to record the maximum amount of useful information including repeat data in the shortest time interval indicated that a continuous-sweep, data-recording mode of operation should be employed. This means that as the sector was pitched through an angle of attack, the test results were continuously recorded at the rate of 1,400 words per second. Nominally, each measurement (i.e., each balance, pressure, temperature, and model parameter) was recorded 50 times per second. A single data point consisted of the average value of 14 recorded measurements of an individual input channel.

In the case of the ablative models, the following procedure was adopted in recording the test results. The ablative components of the model were weighted before and after each run; also, an evaluation was made of the time the model was exposed to the air stream. In addition to weighing the model components, the 3-component force balance was also used to define the model tare weight before and after each model injection into the tunnel air stream. Once the instrumentation was activated, the model was injected into the tunnel at zero angle of attack and then automatically pitched slowly (about 1 deg per second) to a maximum angle of 3 to 4 deg and then back to 0, and to -1 deg, and finally returned to zero angle of attack and immediately retracted. A typical run sequence is shown in Fig. 7. The forward 50 percent of the 4-deg, all-camphor model is compared in Fig. 8 at several times with the all-steel model showing how much the
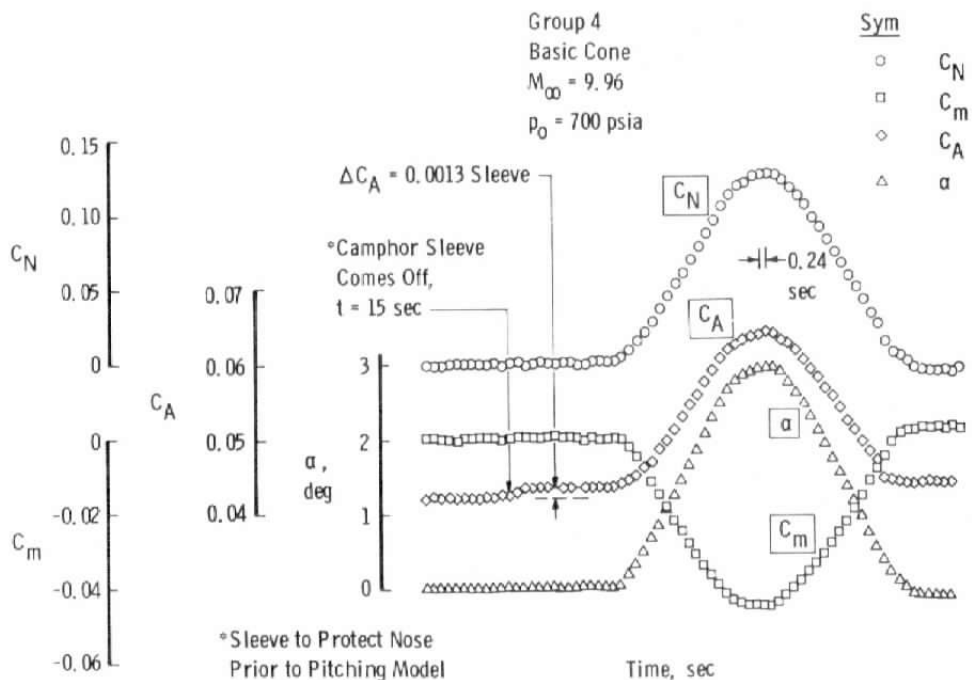
Figure 7. Data versus time for basic cone, $R_N/R_B = 0.05$, $\theta_c = 4$ deg.

Group 3 Metal Model

Group 21, Camphor Model, t = 0

Group 21, Camphor Model, t = 5 sec

Group 21, Camphor Model, t = 15 sec

Figure 8. Forward 50 percent of the basic 4-deg cone, $R_N/R_B = 0.05$,
$p_o = 250$ psia, $T_o = 1,823°R$, $M_\infty = 10$, $a = 0$.

camphor ablated during the run. Since some models were fitted with an ablative sleeve to protect the model nose during the model injection into the air stream, a pause at the beginning of each pitching sequence was needed so that this protective sleeve would ablate and fall free of the model. In most cases, the balance was sensitive enough to confirm by means of the axial-force measurement when the ablative sleeve fell free of the model nose. The performance of the sleeve was erratic, and after a few runs this procedure was stopped. By utilizing the model injection system the ablative sections of the model could be changed in 5 or 10 minutes and data on the new configuration immediately obtained.

The same process was used when data were recorded for the porous mass addition and solid stainless steel model configurations. In the case of the porous models, all model zeros were recorded in the injection tank aft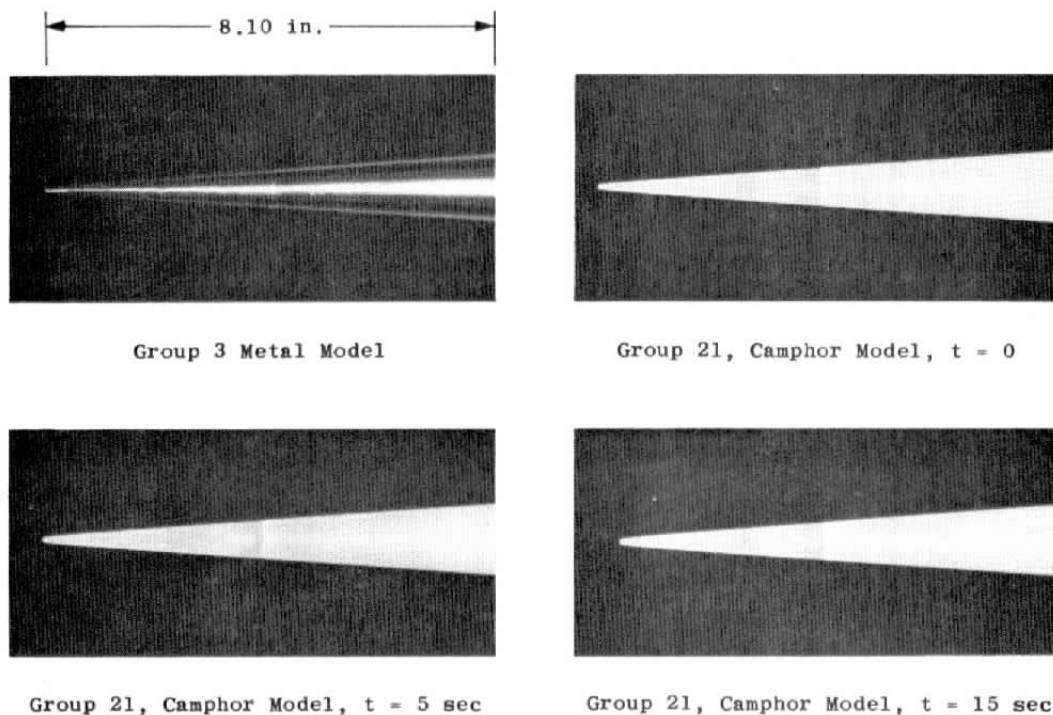er the mass flow rate through the model was established and prior to injection of the model into the air stream. These preloading procedures improved the repeatability of the balance zeros and the reliability of the test results.

The mass flow system shown in Fig. 9 was used to establish prescribed flow rates through the model. Two heat exchangers were required to convert the liquid supply of SF_6 (sulfur hexafluoride) to a gaseous state. The container of liquid SF_6 was placed in a 50-gal drum of water, and then steam was passed through a line in the water bath to heat up the bottle of SF_6 as suggested in the schematic by the item designated "Heat
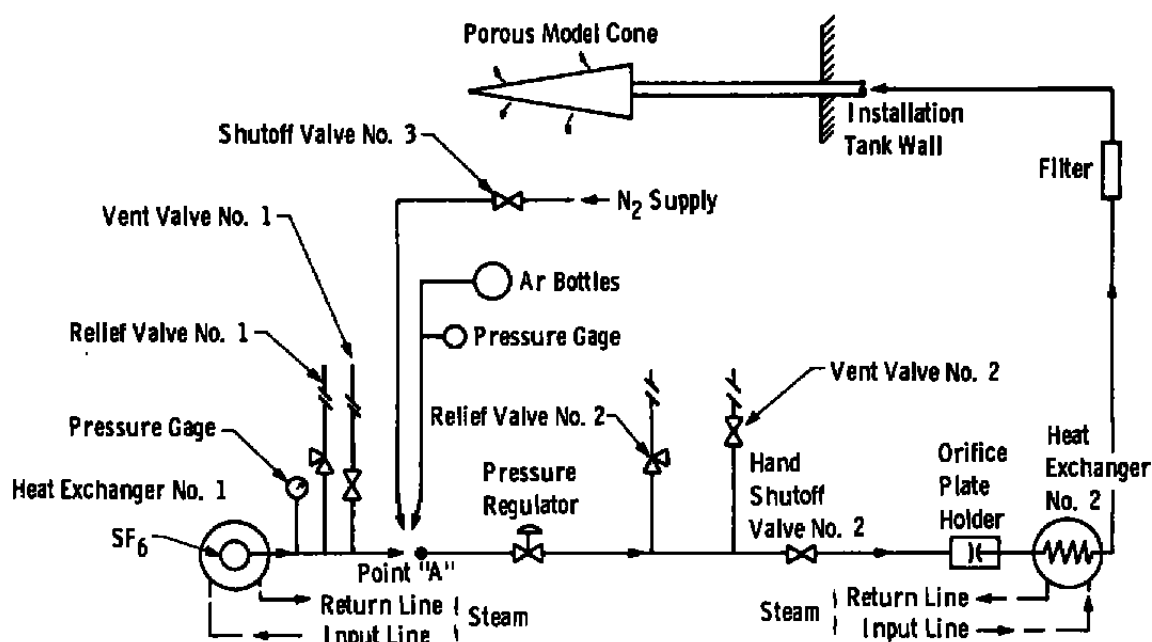

Figure 9. Gas supply system.

Exchanger No. 1." The gaseous SF_6 was metered through a valve, and the flow rate was measured by means of interchangeable 0.013- or 0.026-in.-diam sonic orifices. A second heat exchanger was located in this system to provide additional assurance that the SF_6 remained in a vapor state. As indicated in the figure, either SF_6, argon, or nitrogen could be supplied by making a change in the supply line system at point "A" in the mass flow system.

3.0 ABLATION SIMULATION

3.1 CALCULATION OF MODEL WEIGHT LOSS

Reentry vehicles traveling at high velocities require some sort of thermal protection system to prevent internal damage caused by aerothermodynamic heating. A passive system in which the skin of the vehicle is covered with an ablating material is generally used, especially on the afterbody surfaces of the vehicle. Complex computer codes are required in order to compute the mass loss of a vehicle with a realistic material that has a relatively high heat of ablation. For such materials as teflon and camphor, which have a relatively low sublimation temperature, an "effective-heat-of-ablation" approach can be utilized.

$$H^* = \frac{Z\dot{q}_{o,w}}{(\rho v)_w} \tag{1}$$

where

$$(\rho v)_w = \text{Local mass injection rate at wall}$$

$$\dot{q}_{o,w} = \text{Wall heat-transfer rate with no} \\ \text{blowing or ablation}$$

$$Z = \text{Percent reduction in } \dot{q}_{o,w} \text{ caused by} \\ \text{upstream ablation}$$

$$H^* = \text{Effective heat of ablation}$$

An experimental value of H^* can be determined for camphor by measuring the stagnation recession rate of the camphor models under conditions of interest. Figure 10 gives the "effective heat of ablation" derived from the present experiments compared to some previous data under similar test conditions (see Ref. 1). The data of Fig. 10 will be used to calculate the total mass loss for camphor models tested. and that result will be compared with the measured mass loss.

Rewriting Eq. (1) gives

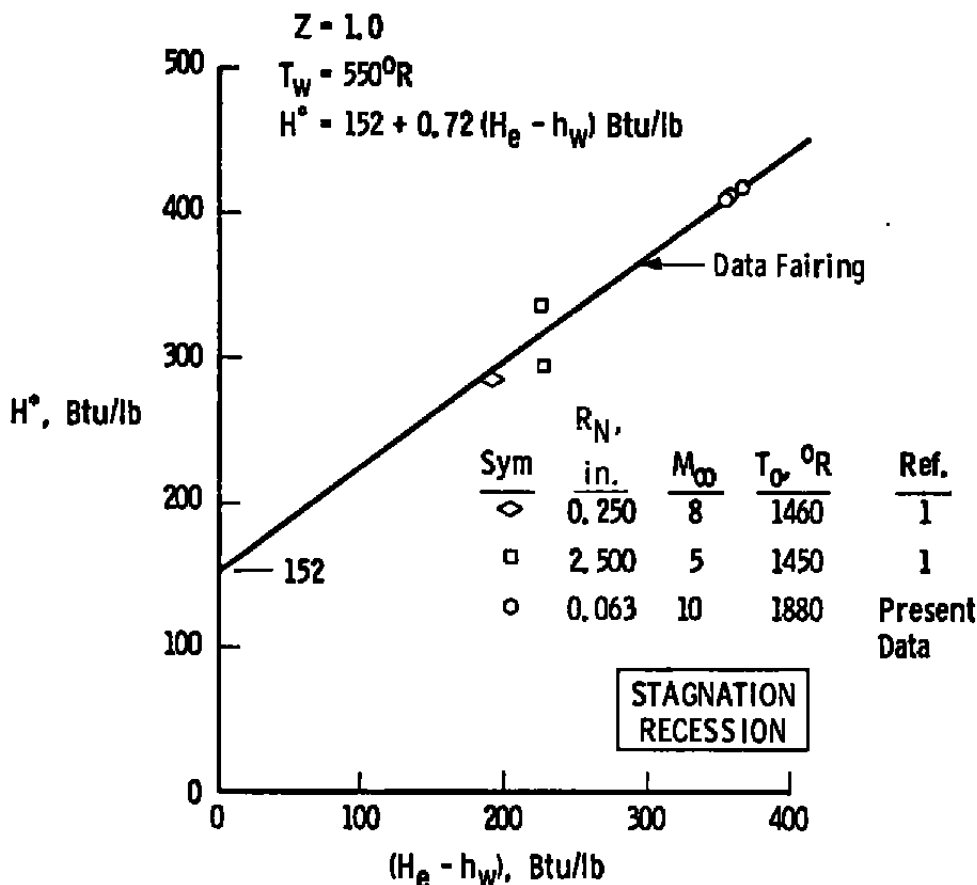$$(\rho v)_w = \frac{Z\dot{q}_{o,w}}{H^*} \tag{2}$$

Figure 10. Experimental heat of ablation for camphor, laminar flow.

It is now possible to calculate and integrate the local mass loss down the body by knowing only H^*, $\dot{q}_{o,w}$, Z, and time. The effective heat of ablation, H^*, is known (Fig. 10), the heat-transfer rate with no ablation $(\dot{q}_{o,w})$ can be calculated (see Ref. 2), and only the upstream influence of ablation on $\dot{q}_{o,w}$ is left unknown.

Figure 11 presents a theoretical analysis of the reduction of local surface heat rates due to upstream blowing for air-into-air. Allowing for changes in the molecular weight between air and the actual model material, the following expression can be derived from the theoretical data of Fig. 11:

$$Z = 1.0 - 0.4073 \left\{ B_o(X,Y) \left[\left(\frac{(MW)_{air}}{(MW)_{gas}} \right) \right]^{1/3} \right\} + 0.0425 \left\{ B_o(X,Y) \left[\left(\frac{(MW)_{air}}{(MW)_{gas}} \right) \right]^{1/3} \right\}^2$$

(3)

where the term $\left[\left(\frac{(MW)_{air}}{(MW)_{gas}} \right) \right]^{1/3}$ follows Eq. (227), pp. 17 and 18 of Ref. 3.
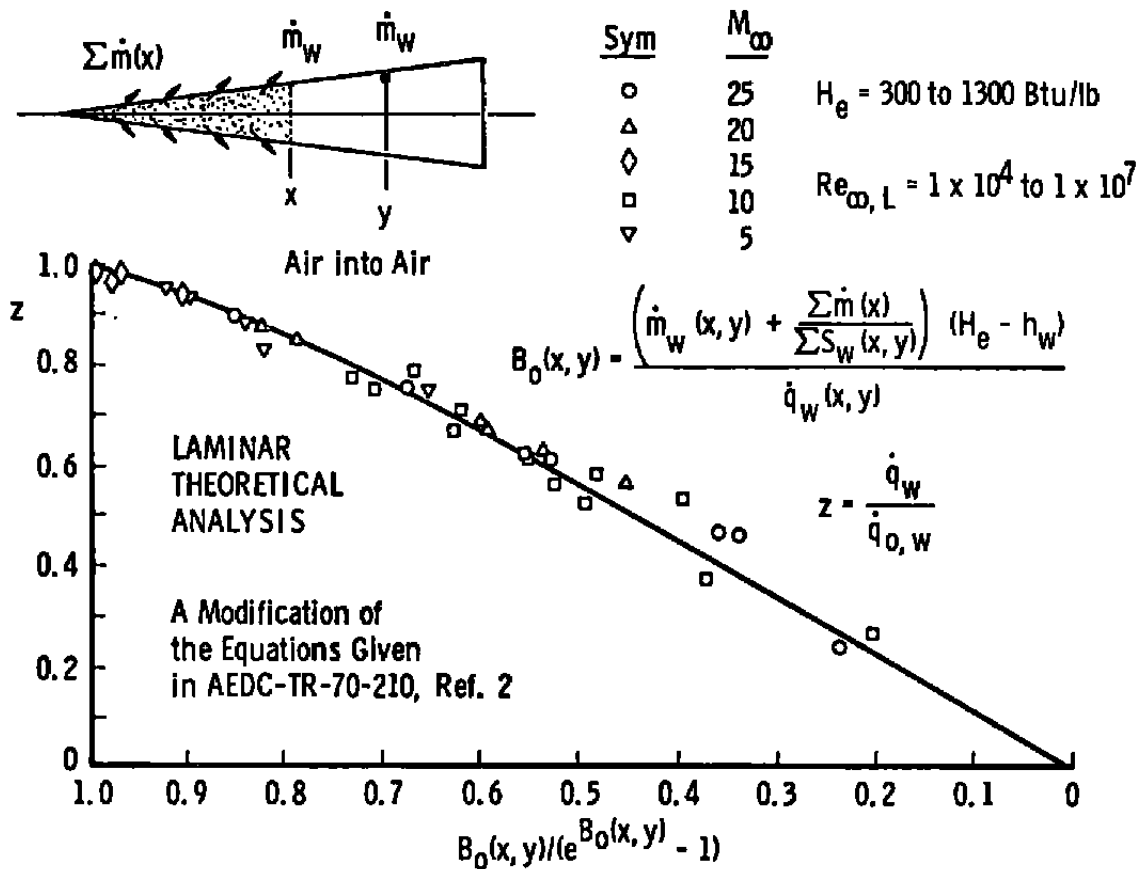
Figure 11. Effect of upstream and local ablation on model surface heat-transfer rate.

A more rigorous analytical treatment of the influence of molecular weight is being made by the use of the Boundary-Layer Integral Matrix Procedure (BLIMP) and the Aerotherm Chemical Equilibrum (ACE) computer codes. However, in the present report Eq. (2) will be utilized as a check against the actual measured mass loss of a given configuration.

Figure 12a shows a comparison between the total measured weight loss and computed weight loss of a series of camphor models over a range of tunnel flow conditions. Excellent agreement is noted which adds validity to the quoted ablation rates given in Section 4.0 for the camphor models. Figure 12b also shows excellent agreement between the computed recession rate and the actual measured rate for three tunnel flow conditions. Since these data were used in the evaluation of H*, the agreement. of course. has to be good.
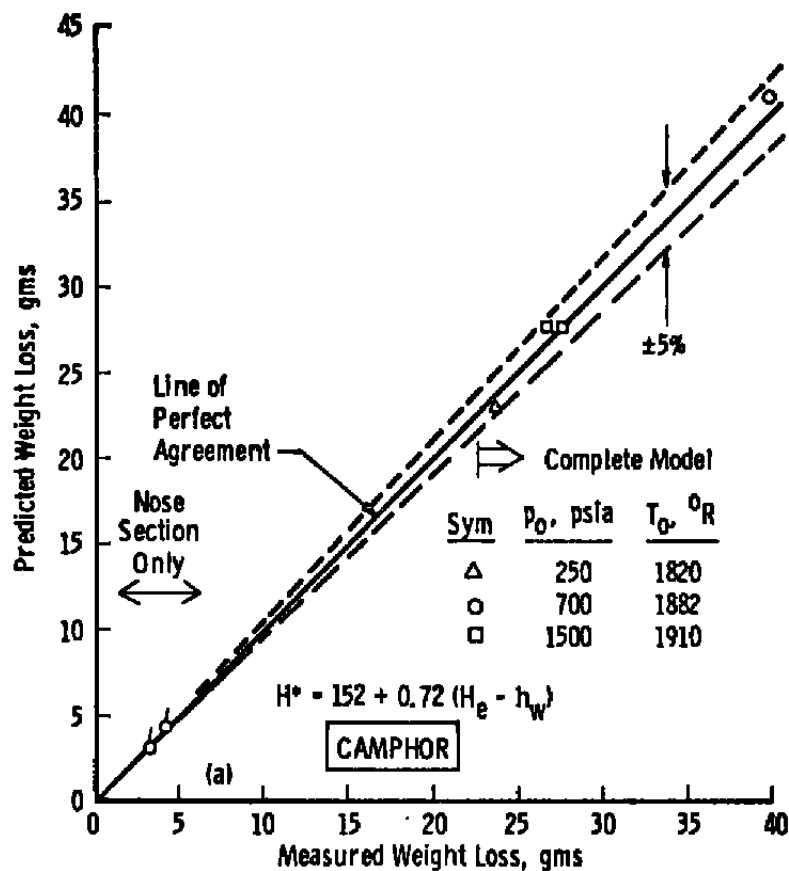
a. Computer versus measured total weight loss
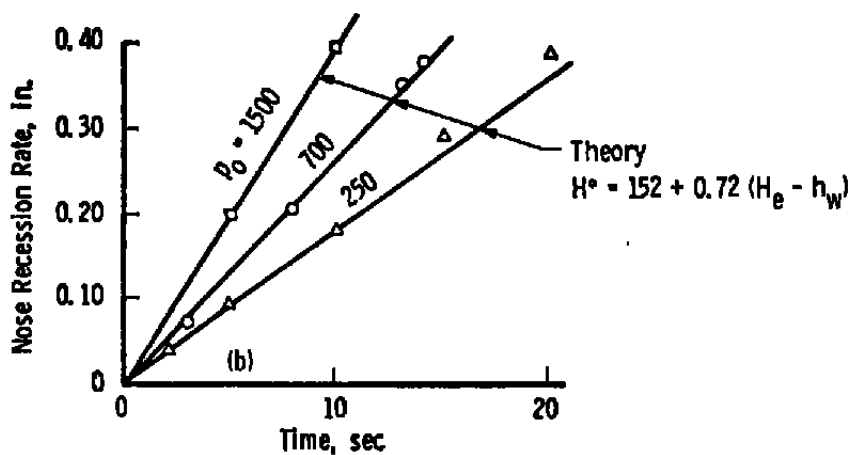
b. Nose recession

Figure 12. Comparison of measured and calculated nose recession
rates and model weight loss.

3.2 SIMULATION PARAMETER

The blowing or ablation rates are normalized by the nonablating heat-transfer coefficient at the end of the body for ease of comparison. Hence the simulation parameter to be used is defined as follows:

$$B_o = \frac{\Sigma \dot{m} (H_e - h_w)}{(\dot{q}_{o,w})_{\frac{x}{L}=1} (S_w)} \qquad (4)$$

Figure 13 presents the computed heat-transfer-rate distribution of the 5-deg sharp cone for the camphor-type distribution (see Fig. 3) and the porous-type distribution compared to a no-blowing case. These calculations are made following the work of Adams in Ref 2. The theoretical reduction in friction drag for a range of blowing rates is given in Fig. 14. The camphor-type mass rates over the model result in a slightly greater reduction in friction drag for the same simulation parameter (B_o). It should be noted that the results of Fig. 14 represent air-into-air blowing using the camphor-type $\overline{\dot{m}_w}$ distribution and blowing distribution from Fig. 3.
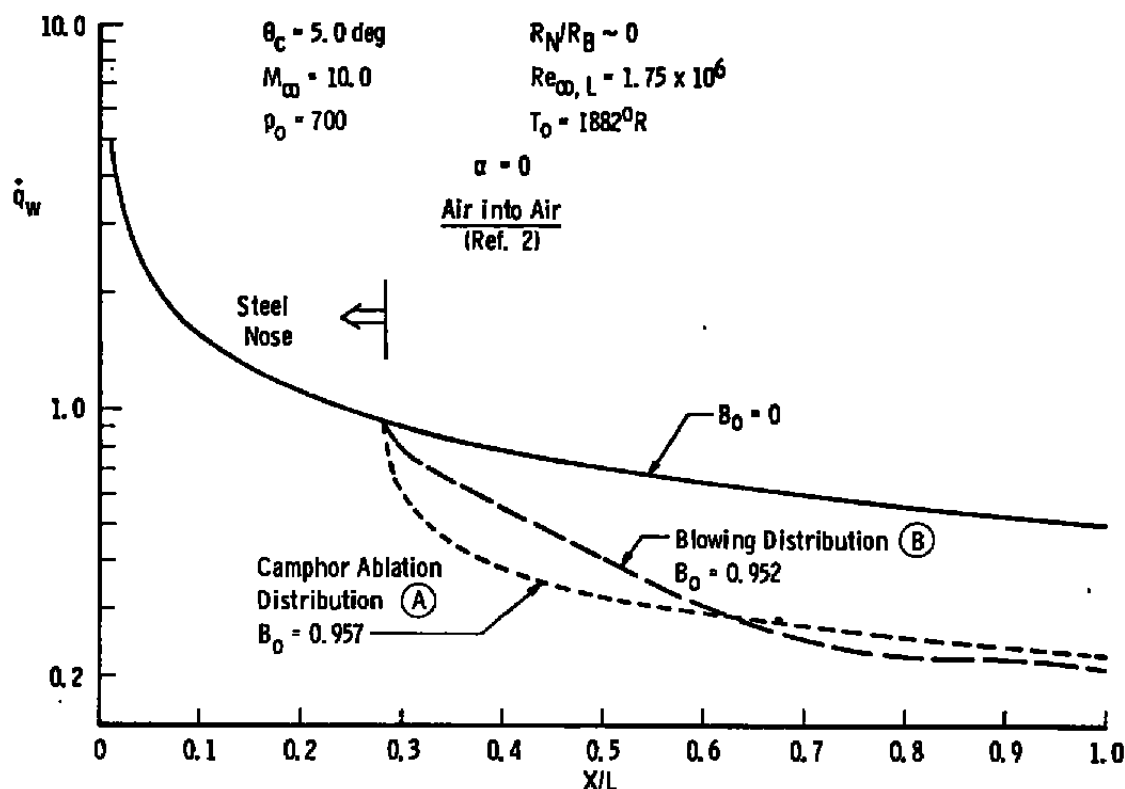

Figure 13. Theoretical reduction of heat-transfer rate on 5-deg cone caused by ablation or blowing.
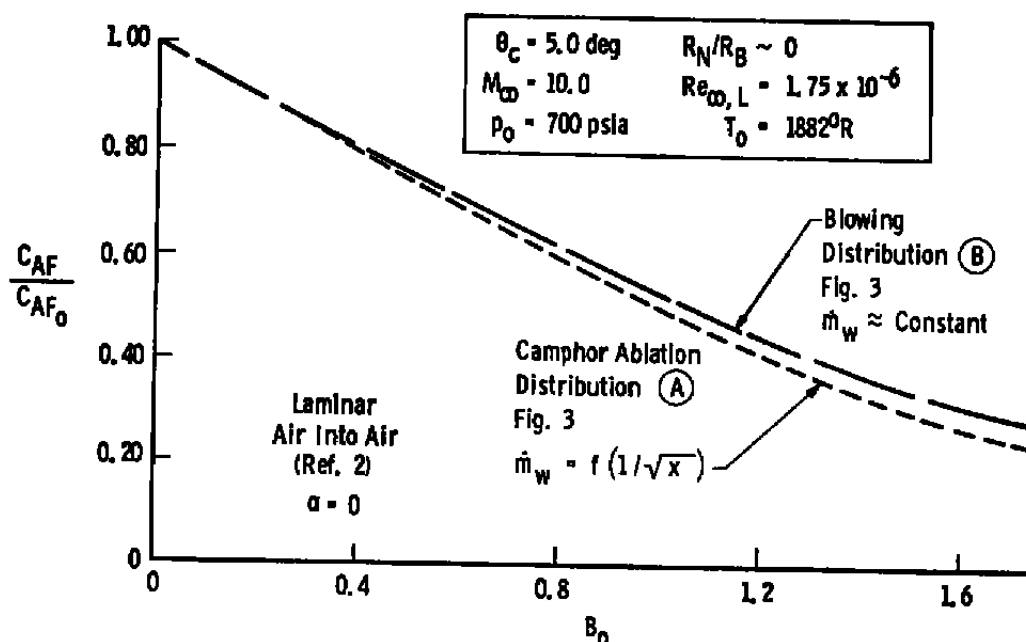
$$\theta_c = 5.0 \text{ deg} \quad R_N/R_B \sim 0$$
$$M_\infty = 10.0 \quad Re_{\infty,L} = 1.75 \times 10^{-6}$$
$$P_0 = 700 \text{ psia} \quad T_0 = 1882^\circ R$$

Blowing Distribution (B) Fig. 3 $\dot{m}_w \approx$ Constant

Camphor Ablation Distribution (A) Fig. 3 $\dot{m}_w = f\left(1/\sqrt{x}\right)$

Laminar Air Into Air (Ref. 2) $a = 0$

Figure 14. Theoretical reduction of friction drag on 5-deg cone caused by blowing.

4.0 RESULTS AND DISCUSSION

4.1 5-DEG SHARP CONE

4.1.1 Transpiration Experiments (SF_6, Ar, N_2)

The basic data for the transpirational cooling experiments are given in Figs. 15 through 17. The data for zero blowing were taken using Model 1 (Fig. 2) in order to keep the porous sintered metal from being exposed to the high stagnation temperature of Tunnel C without surface cooling. Injecting SF_6 through the surface of Model 2 (Fig. 2) moves the center of pressure forward, decreases the normal-force coefficient, and decreases the axial force (see Fig. 15). The boundary layer of the model is undoubtedly "blown" off at the highest blowing rate ($B_0 = 1.578$). The decrease in normal force is most probably caused by higher surface pressures on the lee side of the model because of blowing. The reduction in axial force is caused by the lower model friction drag. The forward movement in the center of pressure may also be partly caused by reducing the friction drag of the model, since viscous effects tend to move the center of pressure aft on the model.

Figures 16 and 17 present the data with argon and nitrogen blowing. The trends are very similar to the SF_6 results, indicating a weak influence of molecular weight on the drag and static stability of the model caused by blowing.
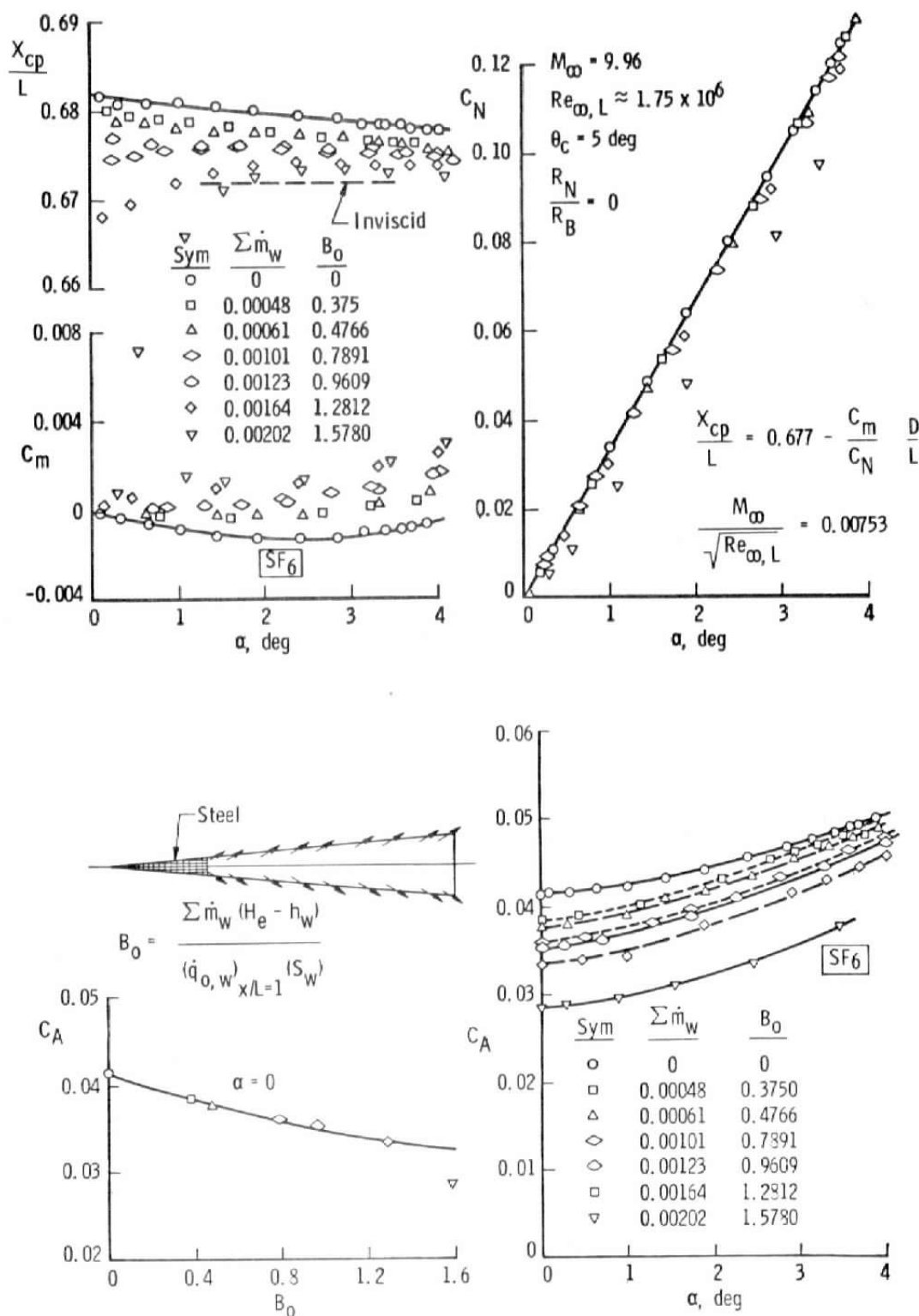
Figure 15. Basic data for sharp 5-deg cone, SF₆ blowing.
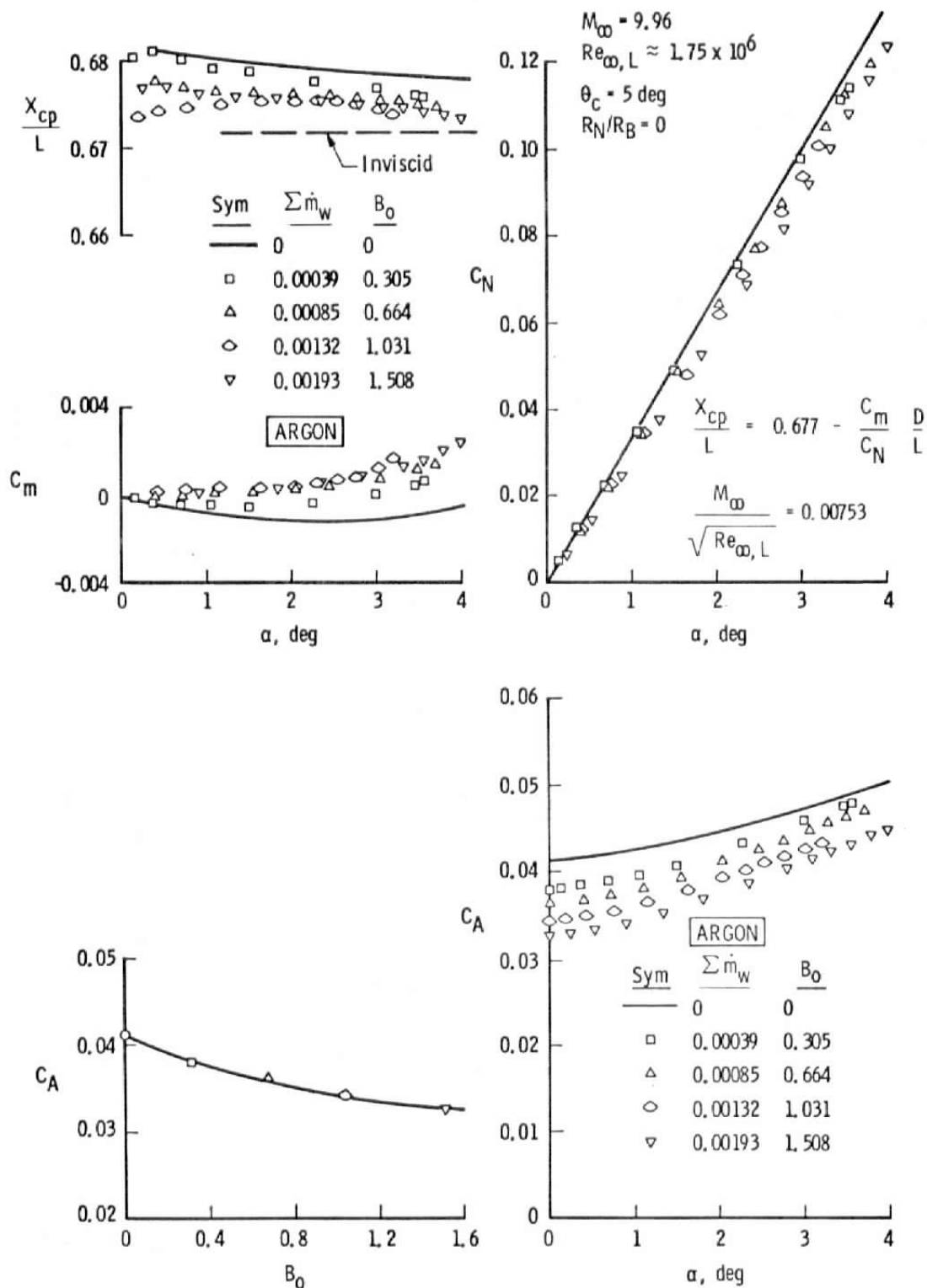
Figure 16. Basic data for sharp 5-deg cone, argon blowing.

21

$M_\infty = 9.96$

$Re_{\infty, L} = 1.75 \times 10^6$

$\theta_C = 5$ deg

$R_N/R_B = 0$

$$\frac{X_{cp}}{L} = 0.677 - \frac{C_m}{C_N} \frac{D}{L}$$

$$\frac{M_\infty}{\sqrt{Re_{\infty, L}}} = 0.00753$$

Sym	$\Sigma \dot{m}_w$	B_0
—	0	0
◇	0.00019	0.148
□	0.00052	0.406
△	0.00086	0.672
◇	0.00109	0.851
▽	0.00200	1.560

NITROGEN

α = 0

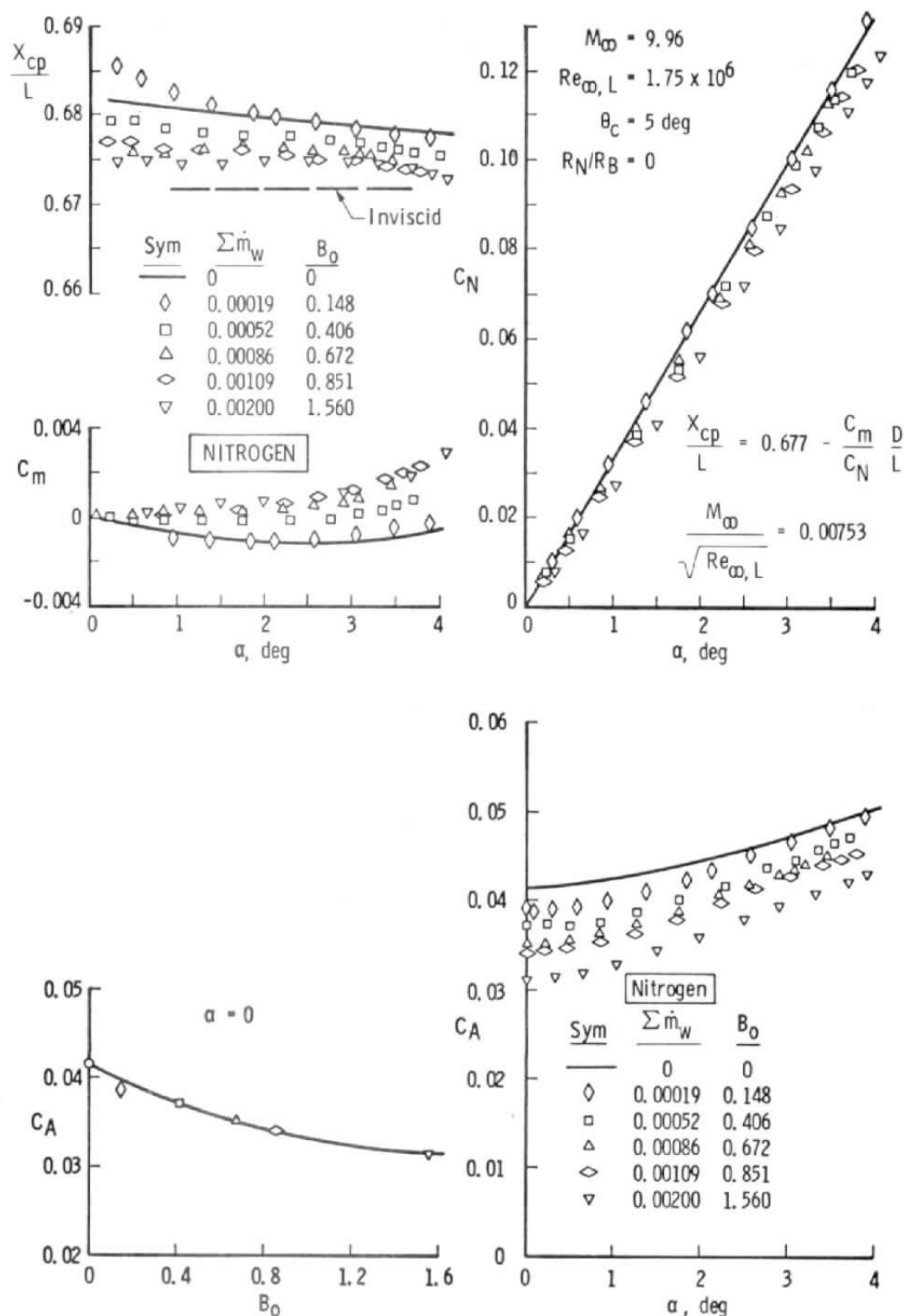| Sym	$\Sigma \dot{m}_w$	B_0
—	0	0
◇	0.00019	0.148
□	0.00052	0.406
△	0.00086	0.672
◇	0.00109	0.851
▽	0.00200	1.560

Nitrogen

Figure 17. Basic data for sharp 5-deg cone, nitrogen blowing.

4.1.2 Camphor Ablation and Comparisons

The effect of camphor ablation on the 5-deg sharp cone is shown in Fig. 18. Data for SF_6 at a similar blowing rate are also shown so that a direct comparison can be made between the two modes of ablation simulation. Camphor ablation causes a greater reduction in C_A, especially at angle of attack, and only a slight forward shift in the center of pressure. Part of the reason for the greater reduction in C_A is most probably a higher "effective" B_o at angle of attack for the camphor model. The reason for the 0.25-percent center of pressure difference could be the difference in distribution, but this is not absolutely clear.
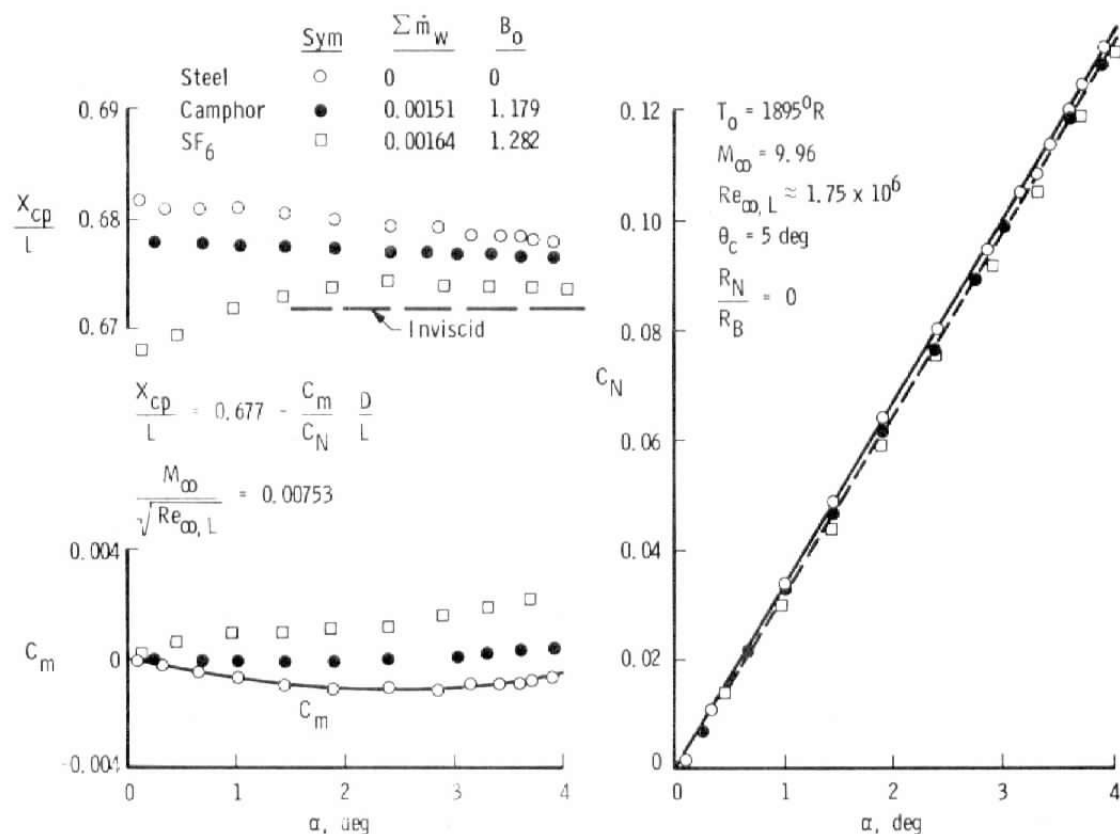

Figure 18. Comparison of camphor ablation and SF_6 blowing.

A summary of the effect of the two modes of ablation simulation is presented in Fig. 19 versus angle of attack and the blowing parameter B_o. The zero angle-of-attack axial-force data show a definite trend with molecular weight. The normal force is reduced in a similar manner by all three of the injected gases and also by the camphor ablation. The molecular weight of the injected gas has no significant influence on the amount of the forward center of pressure shift, and the mode of ablation has only a slight effect, as noted.
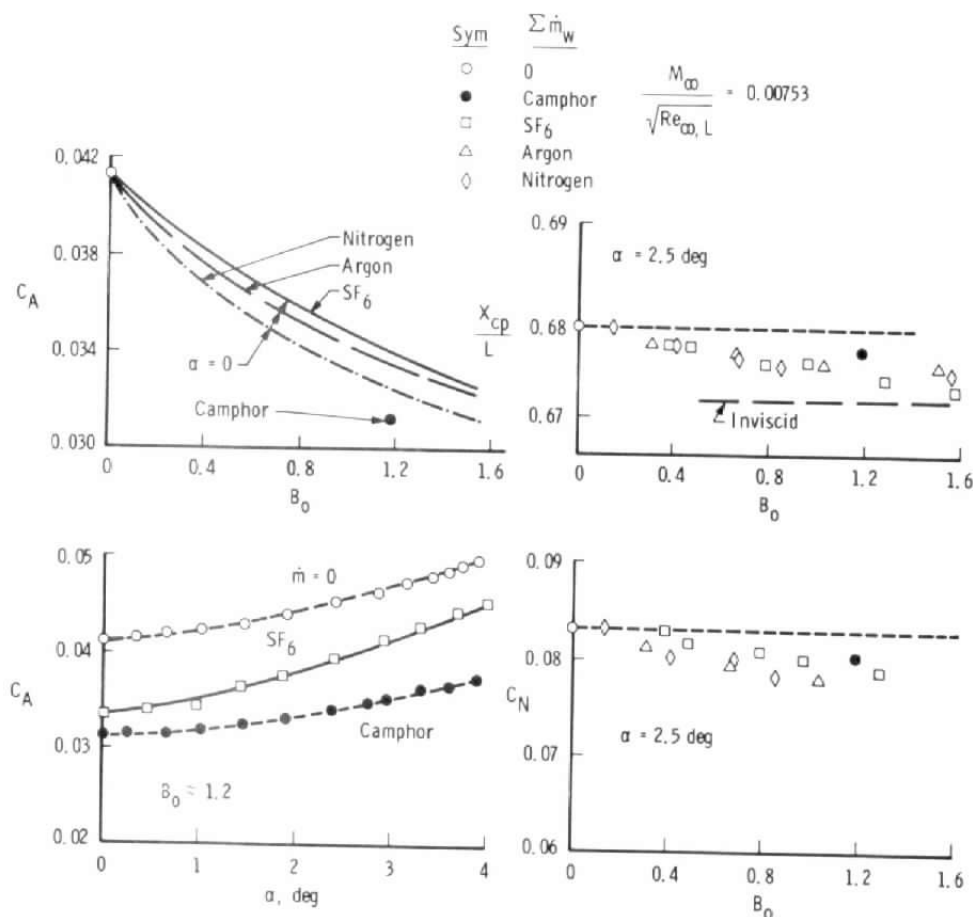
23

Figure 19. Summary of 5-deg cone ablation and blowing data.

4.2 4-DEG CONE

4.2.1 Camphor Ablation and Bluntness Effects

Basic data for the effect of camphor ablation and nose bluntness on the force and moment data of a 4-deg cone are given in Figs. 20 through 22. Details of the cone configuration are given in Fig. 4. The test models were made all camphor, part camphor, or all steel. Data for all-steel and all-camphor models are presented for three test conditions in Tunnel C. These are p_o = 1,500, 700, and 250 psia, with only slight changes in M_∞ and T_o. The quoted bluntness ratio (R_N/R_B) on the all-camphor models is an average value measured during the sweep cycle from enlarged photographs. The total sweep cycle would take about 8 sec with R_N/R_B increasing about 0.004, 0.003, and 0.002 per second for p_o = 1,500, 700, and 250 psia, respectively. Generally, data only for the positive angle-of-attack sweep part of the run at p_o = 1,500 psia were used because of the higher rate of nose ablation.
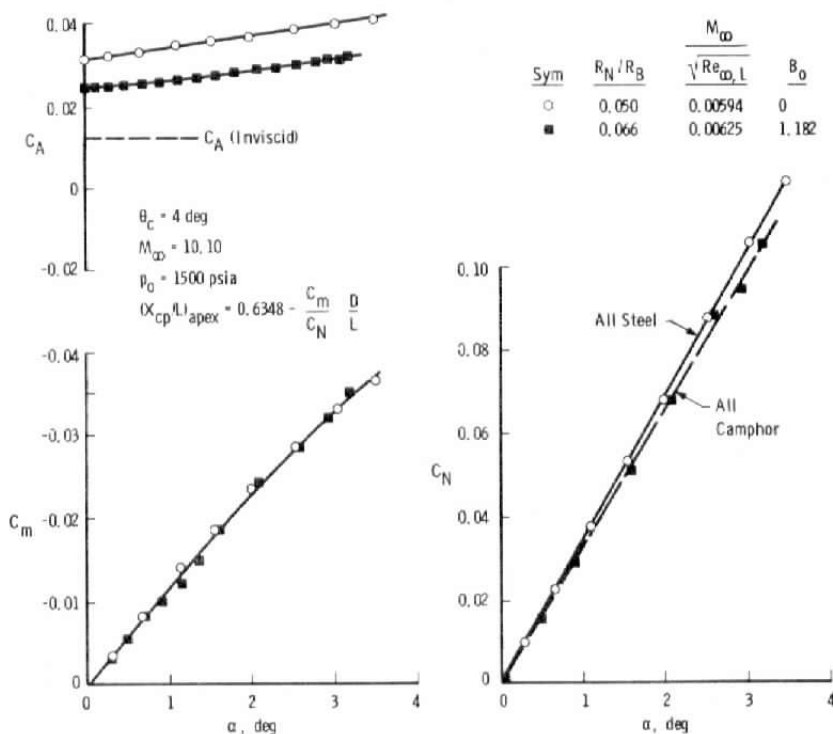
Figure 20. Basic data for 4-deg cone, $p_o = 1,500$ psia.
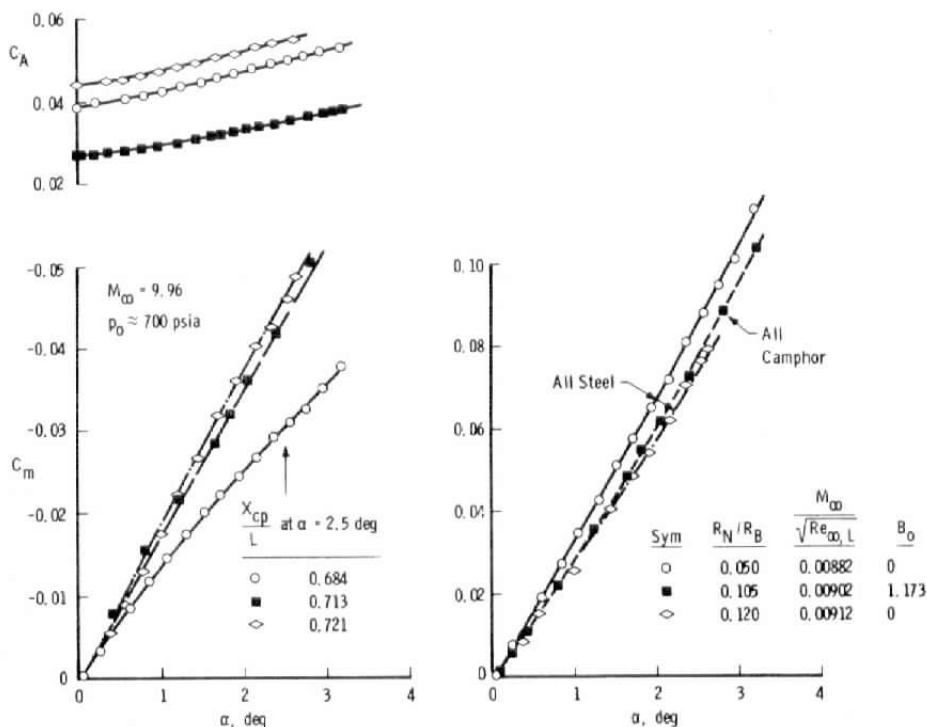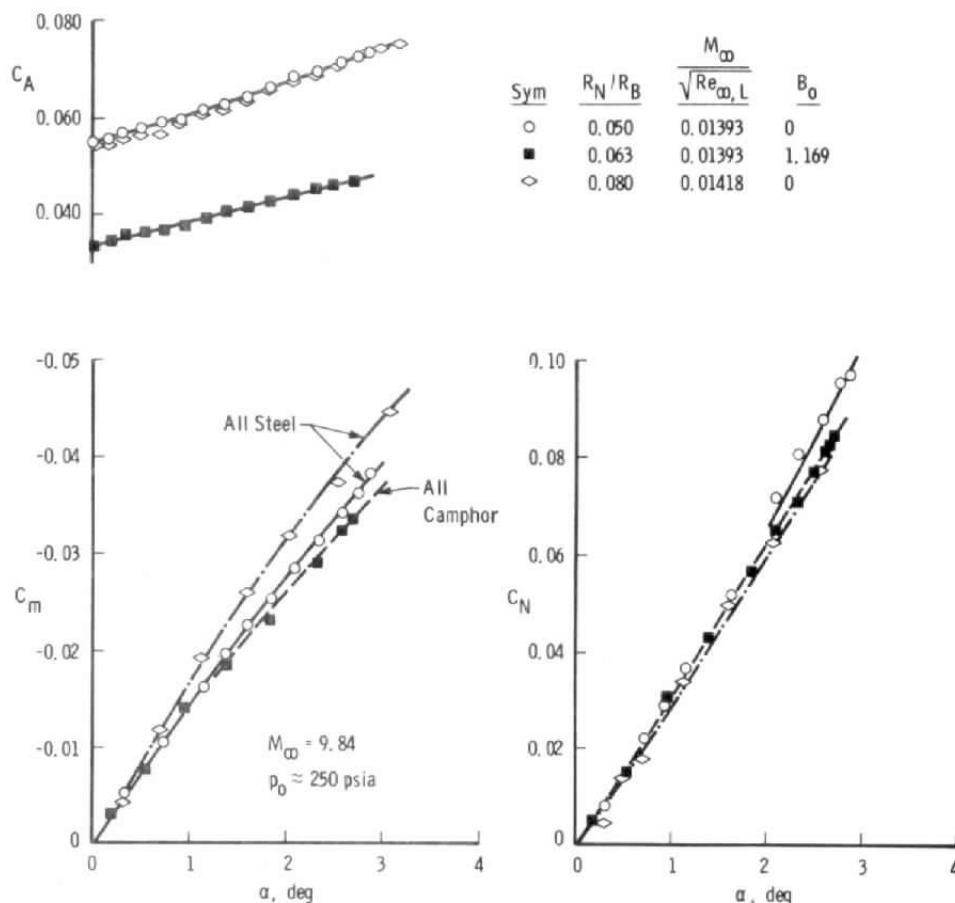

Figure 21. Basic data for 4-deg cone, $p_o = 700$ psia.

Figure 22. Basic data for 4-deg cone, p_o = 250 deg.

Figure 23 presents a summary of the model center of pressure at a = 2.5 deg versus bluntness ratio. Nose bluntness has a significant influence on the model center of pressure, especially in the region between R_N/R_B = 0.05 and 0.10. Hence great care must be taken when data are compared between two similar models. A small forward shift caused by camphor ablation can be noted in X_{cp}/L which supports the data presented for the 5-deg cone in Section 4.1. Also worthy of note in Fig. 23 is the forward movement in X_{cp}/L with decreasing $M_\infty/\sqrt{Re_{\infty,L}}$ suggesting a strong viscous effect. Section 4.2.2 presents additional data showing that this strong viscous influence is real. Figure 24 illustrates the influence of camphor ablation on C_A and C_N of the 4-deg cone. A close inspection of the data will show a similar reduction in friction drag due to camphor ablation on the 4-deg data presented here and the 5-deg data of Section 4.1. No significant reduction in C_N due to ablation is noted. This is not in severe disagreement with the 5-deg data of Section 4.1 since a decrease in C_N of only 3 percent is noted in Fig. 19, which is within the scatter of the data of Fig. 24.
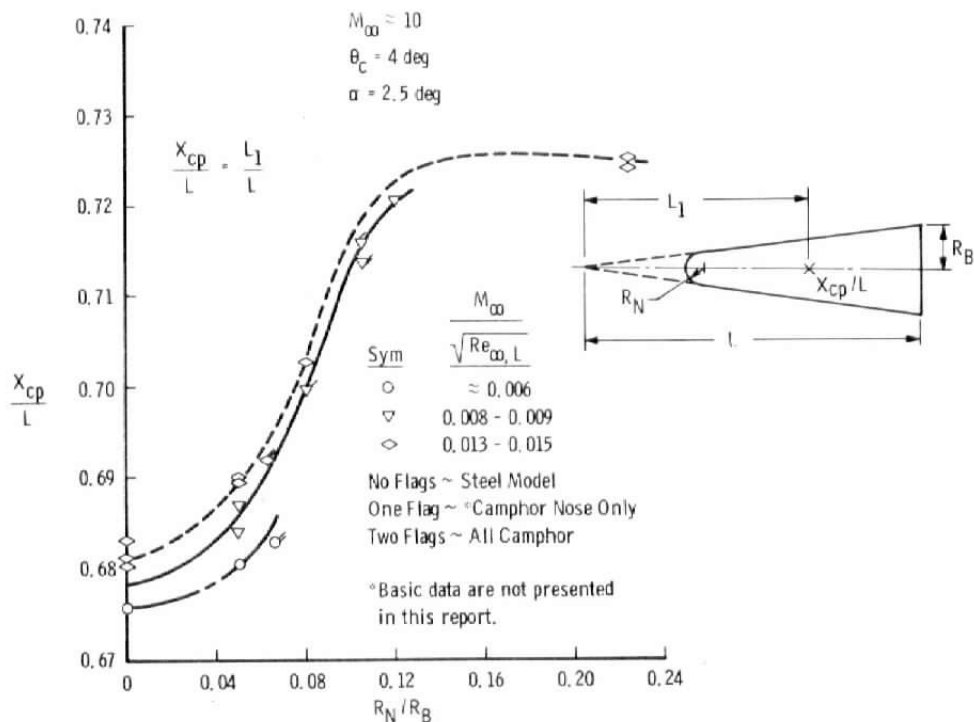
Figure 23. Effect of bluntness on X_{cp}/L of 4-deg cone.
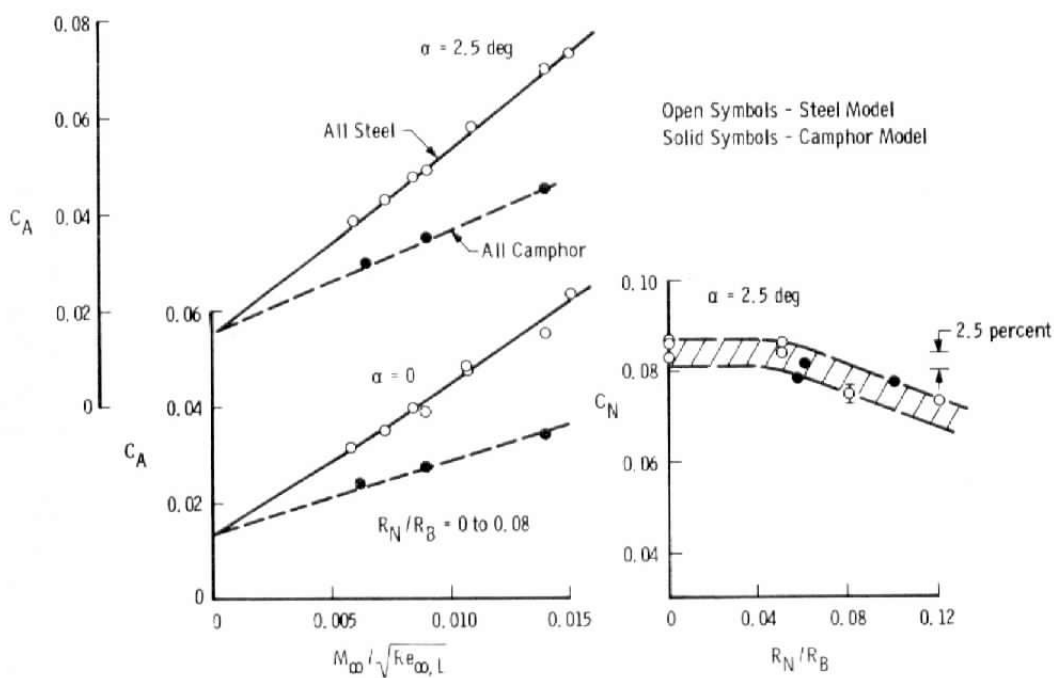
Figure 24. Effect of camphor ablation on C_A and C_N of 4-deg cone.

4.2.2 Viscous Effects

Data for the 4-deg sharp cone are given in Fig. 25 over a free-stream Reynolds number range based on model length from 0.451×10^6 to 3.03×10^6. A significant forward shift is noted in X_{cp}/L as Reynolds number increases while no change is noted in the normal-force coefficient. Note also the significant increase in C_A as $M_\infty/\sqrt{Re_{\infty,L}}$ increases. The center of pressure, X_{cp}/L, at a given angle of attack also correlates with $M_\infty/\sqrt{Re_{\infty,L}}$ and at $a = 3.5$ shows a 1.25-percent aft shift in center of pressure over the inviscid value at the lower Reynolds number tested.

Figure 26 presents data for a slightly blunted ($R_N/R_B = 0.05$) 4-deg cone. The trends are similar to the sharp cone data of Fig. 26 with some added scatter in the X_{cp}/L data.

A summary of the sharp cone X_{cp}/L data is given in Fig. 27 for $a = 2.5$ deg. Figure 27a shows the variation of X_{cp}/L for both the 4- and 5-deg cones with $M_\infty/\sqrt{Re_{\infty,L}}$ indicating a significant viscous effect for these cones. Since ablation or blowing reduces the friction drag, it is therefore reasonable to expect some change in X_{cp}/L. Figure 27b shows that the trend in X_{cp}/L with B_0 follows the reduction in friction drag. The trend with B_0 could, however, change if one had a high amount of forward or aft ablation (see Ref. 4).

Sym	M_∞	$Re_{\infty,L}$	$M_\infty/\sqrt{Re_{\infty,L}}$
○	10.10	3.033×10^6	0.0058
□	9.88	0.874×10^6	0.0106
△	9.84	0.5509×10^6	0.0133
◇	9.81	0.4512×10^6	0.0146

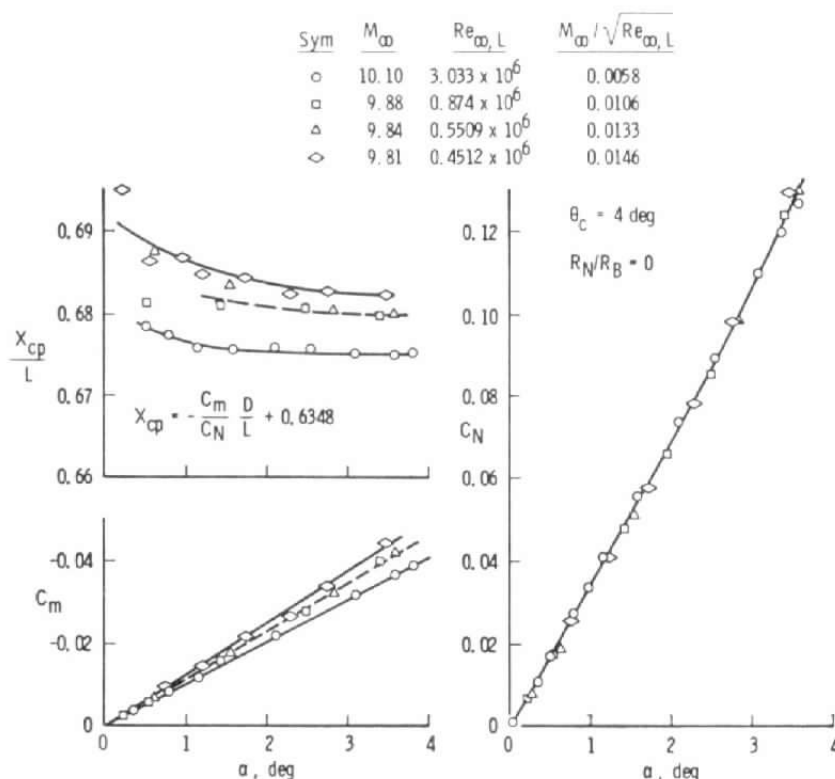$$X_{cp} = -\frac{C_m}{C_N}\frac{D}{L} + 0.6348$$
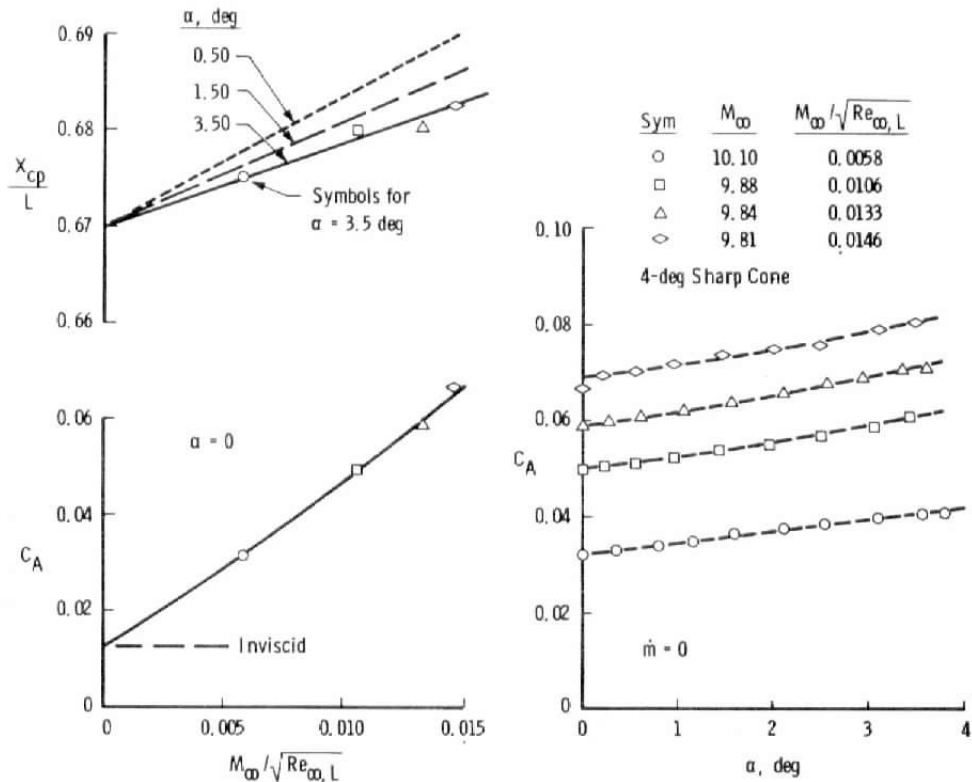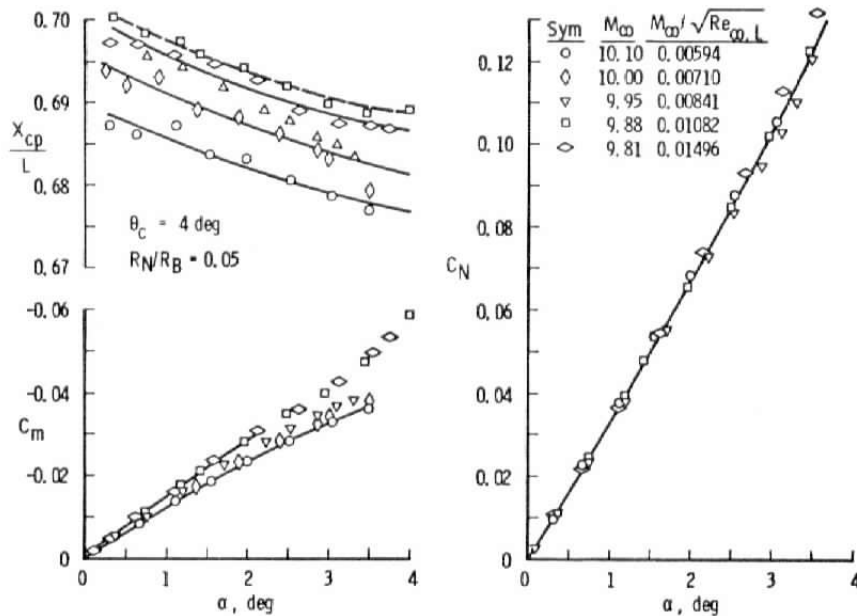
Figure 25. Drag and static stability data for 4-deg sharp cone.

Figure 25. Concluded.

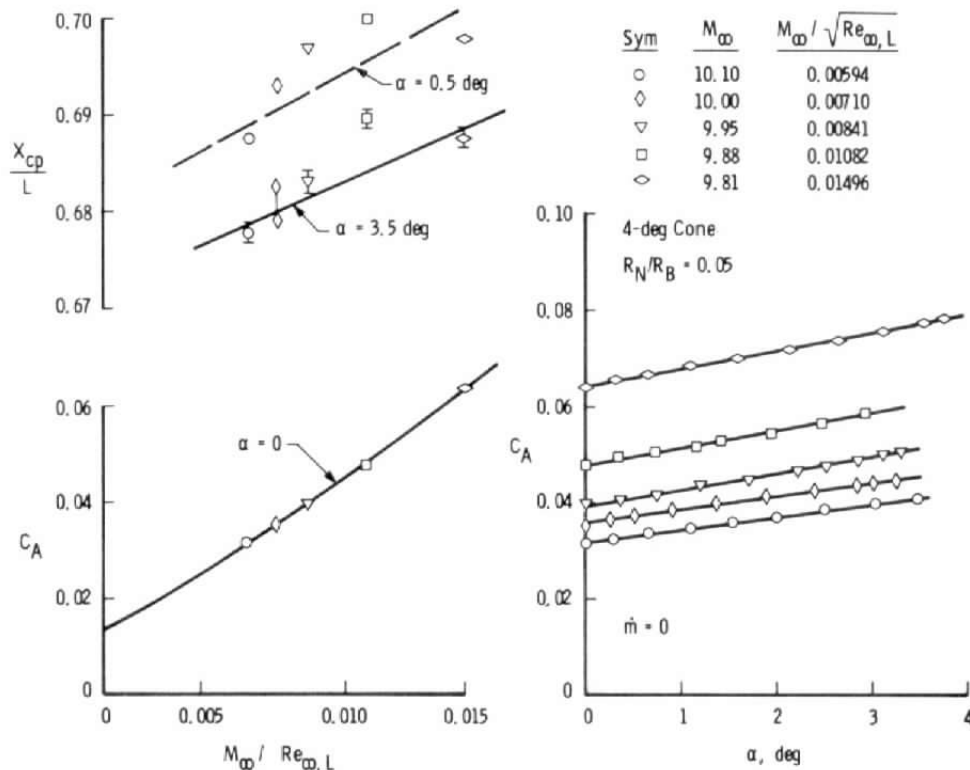Figure 26. Drag and static stability data for 4-deg cone, $R_N/R_B = 0.05$.

Figure 26. Concluded.

a. Viscous effect   b. Ablation effect

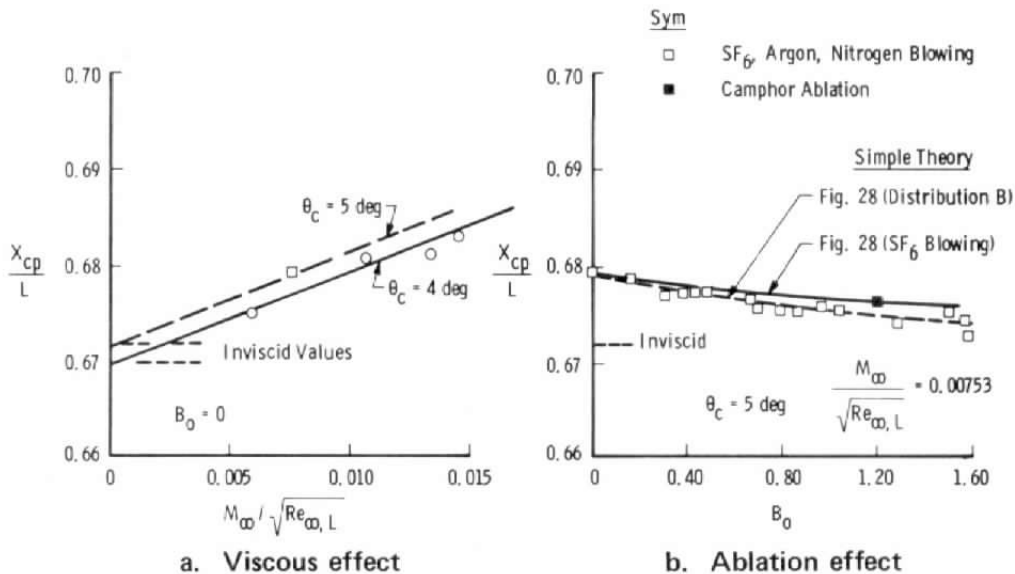Figure 27. Viscous and simulated ablation effects at a = 2.5 deg.

Figure 28 presents a comparison of the theoretical reduction of friction drag (see Fig. 14) and a summary of the porous model data with SF_6 blowing and camphor ablation data at zero angle of attack. As noted before, camphor is more efficient in reducing the friction drag than is blowing.
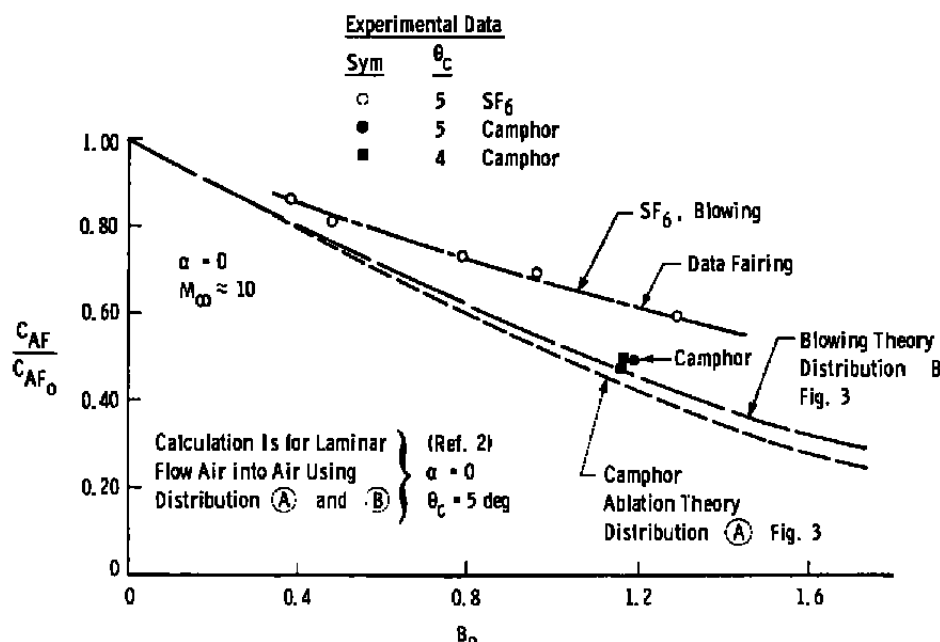
Figure 28. Reduction of friction drag on 5-deg cone caused by blowing and ablation, $\alpha = 0$.

5.0 SUMMARY

Results of the research are summarized as follows:

1. A direct comparison between a model utilizing blowing and one using a subliming low-temperature ablator (i.e., camphor) reveals small but significant differences in the moment and drag characteristics for a 5-deg cone half-angle with a sharp nose.

2. Simulated ablation using camphor is more effective in reducing the laminar friction drag of the sharp 5-deg cone than is blowing through a porous surface using any of the injected gases (i.e., N_2, Ar, or SF_6), especially at angle of attack ($\alpha < 4$ deg).

3. The center of pressure (X_{cp}/L) moves forward on the model with blowing or ablation. No effect of molecular weight is noted in the X_{cp}/L movement. Camphor ablation results in 0.2 percent forward movement at $B_0 = 1.18$, whereas blowing shifts the $X_{cp}/L = 0.4$ percent.

31

4.   The normal-force coefficient is decreased slightly (approximately 4 percent) with both blowing and ablation. Most probably the lee side pressures are increased on the model.

5.   A small amount of nose bluntness (R_N/R_B) shifts the center of pressure rearward by a considerable amount (up to 4.5 percent) below a bluntness ratio of 0.12.

6.   A strong viscous effect is noted on both the sharp and slightly blunted 4-deg cones. The axial-force coefficient is increased with decreasing Reynolds number, whereas the center of pressure, X_{cp}/L, moves aft.

REFERENCES

1.   Baker, R. L. and Crowell, P. G. "Low-Temperature Ablator Nosetip Shape Change at Angle of Attack. AIAA Paper 72-90, AIAA 10th Aerospace Science Meeting, San Diego, California, January 17-19, 1972.

2.   Adams, J. C., Jr. "Eddy Viscosity-Intermittency Factor Approach to Numerical Calculation of Transitional Heating On Sharp Cones in Hypersonic Flow. AEDC-TR-70-210 (AD714058), November 1970.

3.   Rohsenow, W. M. and Hartnett, J. P., editors. Handbook of Heat Transfer. McGraw-Hill Book Company, New York, 1973.

4.   Ibrahim, Shukry K. "Effects of Ablation on the Pitching-Moment Derivatives of Cones in Hypersonic Flow." R-0401-4-4-67 (AD658345), FluiDyne Engineering Corporation, Minneapolis, Minnesota, April 4, 1967.

NOMENCLATURE

A   Model dimension, see Fig. 2

B   Model dimension, see Fig. 2

B_o Blowing parameter, see Eq. (4)

$B_o(X,Y)$ Local blowing parameter, see Fig. 11

cg   Reference center of gravity

C_A Forebody axial-force coefficient, $C_{A_T} + C_{A_B}$

C_{AB} Base drag coefficient, $C_{AB} = \dfrac{[(p_b/p_\infty) - 1]}{\gamma M_\infty^2/2}$

C_{AT} Total drag coefficient

C_{AF} Similar friction drag with blowing or ablation

C_{AF_o} Similar friction drag with no blowing or ablation

C_m Pitching-moment coefficient, $M/q_\infty S_{ref}D$

C_N Normal-force coefficient, $N/q_\infty S_{ref}$

D Model diameter

H^* Effective heat of ablation, Btu/lb

H_e Stagnation enthalpy behind a normal shock, Btu/lb

h_w Wall enthalpy, Btu/lb

L Total model axial length

L_1 Model axial length from apex to model cg

M Pitching moment

M_∞ Free-stream Mach number

$(MW)_{air}$ Molecular weight of test gas

$(MW)_{gas}$ Molecular weight of injected gas or ablated material

$\dot{m}_w$ Local blowing or ablation rate, lb/ft^2-sec

N Normal force

N_2 Nitrogen

p_b Base pressure

p_o Stagnation pressure in reservoir, psia

p_∞ Free-stream pressure

$\dot{q}_w$ Wall heat-transfer rate with blowing or ablation, Btu/ft^2-sec

$\dot{q}_{o,w}$ Wall heat-transfer rate with no blowing or ablation

q_∞ Free-stream dynamic pressure

R_B Model base radius

$Re_{\infty,L}$ Free-stream Reynolds number based on model length

R_N Model nose radius

R_N/R_B Bluntness ratio

SF_6 Sulphur hexafluoride

S_{ref} Reference area, πR_B^2

S_w Total surface area of model

T_w Wall temperature, °R

T_o Stagnation temperature, °R

v Velocity normal to surface

X Axial distance from apex of model

X_{cp}/L Center of pressure defined as $(-C_m/C_N)(D/L) + (cg)$

Z Percent reduction in $\dot{q}_{o,w}$ caused by upstream ablation

α Angle of attack, deg

γ Ratio of specific heats

θ_c Cone half angle, deg

ρ Density

$(\rho v)_w$ Local mass injection rate at wall

$\Sigma \dot{m}_w$ Summation of upstream ablation or blowing, lb/sec